Spin density stabilization of local distortions induced by a monovacancy in δ-Pu

Sarah C. Hernandez,[1] Franz J. Freibert,[1] Richard G. Hoagland,[1] Blas P. Uberuaga,[1] and John M. Wills[2]
[1]*Materials Science and Technology Division, Los Alamos National Laboratory, Los Alamos, New Mexico 87545, USA*
[2]*Theoretical Division, Los Alamos National Laboratory, Los Alamos, New Mexico 87545, USA*

(Received 4 May 2018; published 21 August 2018)

Density functional theory calculations elucidate crystallographic and electronic structural responses of the fcc delta phase of plutonium (δ-Pu) to point defects. Discussed in this paper are responses that vary from a defect exhibiting a local structural instability common in fcc metals to an unusual defect structure that mimics properties similar to the monoclinic α phase. In the prior case, the existence of a self-vacancy when ionic relaxation is allowed induces in the fcc lattice a local tetragonal instability in nearest-neighbor atoms, slight electronic charge increase, and a spin-density decrease. However, in the latter case, after ionic relaxation, the defect is not recognizable as the structure of a vacant site common to many simple fcc metals, but is a complex extended defect involving neighboring atoms to collectively exhibit loss of lattice symmetry through formation of short Pu-Pu bonds and associated narrow bands at the Fermi energy. Partial density of states (PDOS) indicates that these narrow bands form as spectral weighting from the less energetic $6d$ electronic states is shifted to the $5f$ electronic states by means of the spin density, which occupies states at the Fermi energy. The PDOS of a $5f$ system exhibiting narrow bands at the Fermi energy is associated with the formation of an unusual defect structure in the lattice.

DOI: 10.1103/PhysRevMaterials.2.085005

I. INTRODUCTION

Knowledge of point defects in crystalline materials, including formation energies and migration energies, has historically originated in irradiation studies of thermodynamics, lattice structure, and electronic structure experiments. In cryogenic temperature experiments, the irradiation induces a cascade of defects, including vacancy-interstitial pairs (known as Frenkel pairs) and aggregates of the same, resulting in point defect damage in the lattice, which are quenched and thus accumulated, as there is insufficient thermal energy to assist in lattice recovery. For most materials, the final fate of these defects may be recombination/annihilation of the pair or it may be the evolution of more complex defected structures. This depends on important kinetic parameters such as temperature, time, exposure dose, and dose rate. Therefore, controlling temperature conditions enables restraints of the kinetic reactions to relatively long-term effects in the lattice, where exploring the origins lies in instantaneous processes. In many experimental studies, cryogenic irradiation damage accumulation is typically followed by isochronal annealing studies (i.e., methodical annealing with ever-increasing temperatures), which monitor the evolution of various point defect populations thermally driven to become further complicated structures (e.g., vacancy clusters) or to dissociate and annihilate as the material seeks recovery of the lattice towards a state that is relatively close to the perfect lattice [1].

For most metallic elements, external irradiation experiments form the basis of understanding the formation and recovery of point defects. In plutonium (Pu), the most common are produced via a roughly 5-MeV α-decay process. For Pu crystalline solids, the α-decay process introduces damage to the crystal lattice and is largely associated with the approximately 86-keV recoil energy of the ejected uranium atom. The resultant cascade of defects has been calculated via molecular dynamics to have a maximum of over 4000 equivalent Frenkel pairs that stabilize after recombination-annihilation within 40 ps to a remaining 2000 Frenkel pairs [2–4].

Much of our knowledge about the primary damage state in irradiated materials comes from molecular dynamics simulations. To date, there has not been an *ab initio* developed interatomic potential for Pu. Molecular dynamics modelers have employed modified embedded atom method (MEAM) interatomic potentials fitted to only a limited number of experimental data values, such as lattice constants and elastic constants [5]. The MEAM potential has undergone further parametrization to compare to experimental results for stacking fault energy and elastic constants, but there still exists some discrepancy between the theoretical and experimental results [6,7]. Therefore, in order to improve atomistic modeling capabilities and extend the timeframe of damage kinetic evolution further in Pu, one must examine with more fundamental approaches, such as electronic structure calculations of the properties of defects that can both aid in understanding the behavior of radiation-induced defects as well as provide crucial information for improving interatomic potentials.

Why is Pu so unique? The nature of the $5f$ electrons of elemental Pu strongly influences the internal energy, giving rise to six allotropic phases at ambient pressure. Further, Pu is unique among the actinides, known to lie at the boundary of delocalized and localized electrons in the actinide series. The significant 25% volume increase between the room-temperature monoclinic α-phase and the high-temperature fcc δ-phase has been hypothesized to be due to the presence of magnetic moments [8]. In other actinide systems partially filled $5f$ electronic valence bands are highly correlated with conduction electron bands, with these correlations often manifesting themselves as ordered, localized magnetic moments, however not in δ-Pu. Stabilization of δ-Pu by substitutional

gallium (Ga) is well known for its anomalous lack of magnetism [9]. Recent density functional theory (DFT) calculations revealed that the $6d$ electrons hybridized with the Ga solute $4p$ electrons and Ga strongly desires a fully coordinated nearest-neighbor (NN) shell (12 Pu atoms) that is locally contracted [7,10]. The computational tools and capabilities of DFT are well known to contribute to the theoretical understanding necessary to interpret the behavior of defects in the δ-Pu lattice [7], and elucidate some very intriguing behaviors that may be related to experimental observations [11,12]. However, a multiscale model would still be necessary to fully compare to the length and timescales of experimental work.

Only recently have fluctuating magnetic moments been observed in Ga stabilized δ-Pu via inelastic neutron scattering and new questions regarding the correct theoretical model (i.e., density functional theory versus dynamical mean field theory) necessary to realistically simulate δ-Pu have arisen [12–17]. Furthermore, McCall *et al.* has shown that radiation damage does induce localized magnetic moments ($\sim 0.05\,\mu_B$/atom) that are observed as large Pauli susceptibilities in δ-Pu, which indicates narrow bands at the Fermi surface [18]. This temperature-dependent magnetic susceptibility arises from self-damage without measurable distortion of conduction bands. In time, δ-Pu susceptibility exhibits a contribution changing proportionally to the number of α decays implying a non-Fermi-liquid behavior and a disordered Kondo model from disorder-driven interactions coupling local moments with the conduction electrons.

Thus, there is clearly some correlation between defects and the magnetic structure in Pu. In this paper, we use density functional theory to examine the properties of one defect, the monovacancy, in δ-Pu. We find that the ground-state structure exhibits a reduced symmetry reconstruction, stabilized by the local magnetic structure. This defect and the local distortion exhibits a structure very different from that of typical fcc metals, and this is most likely due to the physics underlying the room-temperature α-phase stabilization.

II. COMPUTATIONAL METHODOLOGY

All calculations here were performed using the projector-augmented-wave method [19] as implemented in the Vienna Ab initio Simulation Package [20–23] and the Perdew-Burke-Ernzerhof formulation to the generalized gradient approximation for the exchange-correlation functional [24,25]. We employed a $3\times3\times3$ fcc lattice supercell (108 inequivalent Pu atoms) and a spin-polarized antiferromagnetic (AFM) arrangement is applied to all Pu atoms within the cell. The value for each atomic spin moment within the arrangement is based upon a partially filled $5f$ (i.e., $5f^5$) valence shell as determined for AFM stabilized δ-Pu [8]. The partially filled $5f^5$ shell agrees with experimental measurements such as electron energy-loss spectroscopy, photoemission spectroscopy, and x-ray-absorption spectroscopy [26]. Although magnetism of δ-Pu is complicated [9], and recent experimental and theoretical studies have given newfound information on this subject [12–14], an AFM order provides comparable structural properties to experimental data [10]. The strength of magnetism (AFM arrangement in particular) in the modeling of the allotropic phases of Pu is in agreement with experimental structural and energetic results, as it allows a continuity of electronic structure for these phases and the individual electronic valence states composed of each phase of Pu [27]. It has also been previously reported that a disordered magnetic structure for δ-Pu will induce a more complex interaction field around a Pu vacancy due to the variations of the local spin moment [28]. This behavior is of fundamental importance to our study of defects in Pu as it enables a reliable theoretical treatment of these entities, as local perturbations from the defect allow the system to undergo necessary local distortions for each defect case within the δ phase. It has been computationally observed that the addition of spin-orbit coupling (SOC) and orbital polarization (OP) for δ-Pu decreases the spin moment for a Pu atom from $5\mu_B$ to $3.5\mu_B$ which indicates that spin polarization compensates for the physics related to SOC and OP corrections [29]. Therefore, due to this previous finding and the challenging effort of modeling monovacancies in δ-Pu, we have chosen not to include SOC and OP corrections in this paper.

It has been determined that at this level of theory unalloyed δ-Pu is mechanically unstable at 0 K as observed by an induced c/a tetragonal distortion [30,31]; however, it is thermally stable above ambient temperatures and the addition of Ga into the δ-Pu matrix will decrease the tetragonal distortion [32]. According to x-ray-diffraction experimental results at low temperatures, the cubic phase is retained for stabilized δ-Pu bulk [33]; thus, for simplicity, all calculations preserved the cubic symmetry (i.e., no tetragonal distortion was imposed). Volume optimization of the cubic structure yielded a lattice constant of 4.524 Å, a 2.5% difference from the room-temperature experimental lattice constant (4.637 Å) [34]. Results include relaxation of only the ions, including ions located at the periodic boundary, while maintaining a fixed volume of the structure at the theoretical lattice constant of the perfect supercell. This "dilute limit" method mimics the case of a defect in an "infinite" bulk system [35]; with intentions of a large enough supercell there would be no lattice distortions communicated through the supercell boundaries. Computational parameters include a kinetic-energy plane-wave cutoff of 500 eV, Γ-point k-point mesh, self-consistent electronic relaxation energy convergence of 1×10^{-5} eV, and ions that are relaxed until the Hellmann-Feynman force on each ion is less than 0.01 eV/Å.

III. RESULTS

For this model of δ-Pu, lattice stability is extremely sensitive to defects with just a small perturbation to the lattice, and the fcc lattice may adopt local distortions. Some defects have been calculated to induce short Pu-Pu bonds similar to the room-temperature monoclinic α phase [7]. The model response highlights the disruption of the AFM atomic spin moment used to stabilize δ-Pu within DFT against the local spin moment loss and the influence of magnetic exchange interactions [26]. In this framework, a classical monovacancy is defined as a vacancy at a lattice site, which in most fcc materials will cause a spherically symmetric local volume collapse around the vacancy. Formation energies (E_f) for a monovacancy are

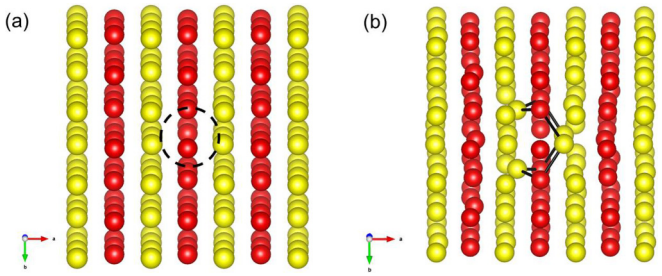

FIG. 1. Final relaxed structures for (a) tetragonal vacancy and (b) monoclinic vacancy. Yellow Pu atoms are spin-up and red Pu atoms are spin-down. Short Pu-Pu bonds are shown in black. Visualizations are from VESTA [38].

calculated by

$$E_f = E_{\text{mono}} - \frac{n-1}{n} E_{\delta-\text{Pu}} \tag{1}$$

where E_{mono} is the total energy of the lattice with defect, n is the number of Pu atoms in the supercell, and $E_{\delta\text{-Pu}}$ is the total energy of a pure δ-Pu lattice with no defects.

In the dilute limit for δ-Pu, we have calculated that a monovacancy exhibits a formation energy of 1.23 eV and causes the nearest-neighbor atom shell to contract approximately 10.36% [7]. Unsurprisingly, there is also no significant long-range disorder observed in the lattice atoms. In Fig. 1(a), the removal of a Pu atom that is spin down (red atom) breaks the symmetry of the AFM arrangement along the [100] direction and the total magnetization of the Pu ions in the supercell no longer sums to 0 μ_B/atom but 0.047 μ_B/atom. Furthermore, vacancy adjacent spin-down atoms exhibit a slight displacement toward the vacant site collectively as a local tetragonal distortion reminiscent of the AFM stabilized δ-Pu mechanical instability against a lattice tetragonal distortion [24]. This tetragonal distortion leads to four short bonds between NNs of length 3.048 Å all in the vertical plane containing the vacancy. When compared against bonding out of a vertical plane of length 4.524 Å, this gives a c/a axial ratio of 1.485, which is nearly the c/a axial ratio of 1.5 resulting from mechanical instability of the AFM structure observed in δ-Pu for other DFT calculations as argued from its low shear elastic modulus [26]. Although in most simple fcc metals, such as copper and aluminum, the classical monovacancy with a spherical distortion would be the ground state for a monovacancy [36], in δ-Pu this is not the case. This type of monovacancy will hence be known as a tetragonal vacancy. Freibert *et al.* discussed the interpretation of historic bulk density, thermal expansion, and x-ray-diffraction experimental data on stabilized δ-Pu and considered that self-irradiation and mechanical damage induced by point defects exhibit a tetragonal distortion [37].

With further relaxation of the ions and with a slight perturbation of the surrounding atoms around the vacancy (an atom slightly off the lattice site), a lower ground-state monovacancy is discovered with a formation energy of 1.08 eV [Fig. 1(b)]. This is a 0.15 eV decrease in energy compared to the tetragonal vacancy in the lattice. The distortion around the monovacancy induces short Pu-Pu bonds where the participating Pu atoms in these distortions form adjacent bonds to opposite spin configurations, i.e., a short bond is formed between two Pu atoms that are spin antiparallel. This response suggests the formation of spin-antiparallel pairs, which brings the lattice atoms surrounding the vacancy closer to a local nonmagnetic configuration (net magnetic moment is 0.094 μ_B/atom), thus forming a localized monoclinic structure within the δ matrix [8]. Hence, this vacancy type will be known as a monoclinic vacancy. The final ion relaxed configuration yields an increase of the net magnetic moment for the Pu ions of 0.056 μ_B/atom, where this increase is in both the $6d$ and $5f$ magnetic contribution. The net total magnetic moment induced in the supercell due to a vacancy is similar in magnitude to the McCall *et al.* measured value of a magnetic moment of 0.05 μ_B/atom that forms due to radiation damage [18].

To investigate the uniqueness between these two different types of monovacancies, starting from a perfect lattice the defect is introduced and after ionic relaxation the atomic rearrangements produce a displacement field that provides certain insights relevant to the underlying bonding symmetry of these vacancies within the AFM stabilized δ-Pu. For example, in many simple fcc metals, the displacement field in the lattice surrounding a vacancy is spherical, and the radial displacement component is proportional to $1/r^2$ (i.e., $u_r = \frac{\delta v}{4\pi r^2}$), while the tangential components are both zero [39]. The proportionality constant, δv, is a property of the defect and, in the case of a vacancy, is the dilatation of the lattice on introduction of the vacancy. However, in the case of fcc Pu, we find much more complex displacement fields associated with vacancies in general.

In Fig. 2 the displacement field in the computational cell is shown in terms of vectors whose length and orientation is defined by $\mathbf{v} = w[u_x, u_y, u_z]$, where w is a scale factor, and the origins of the vectors are at the initial atomic coordinates. In this case the vacant site is at [0, 0, 0] corresponding to the tetragonal vacancy case, and the scale factor is 10. It is fairly clear that the displacement field is not uniformly spherical, but instead consists of four large displacements in the yz plane containing the vacancy and smaller displacements elsewhere. The largest displacement vectors are directed at the vacant site. Furthermore, the z components of the displacements of atoms that are NNs of the vacancy in the yz planes containing the vacancy and the two parallel adjacent planes are essentially zero.

Many of the NN bond lengths in this model have decreased although by a relatively small distance. Those displacements associated with bonds that have decreased by more than 0.1 Å are also shown in Fig. 2. Clearly, the largest decrease in NN bond lengths is associated with atoms confined to the (100) plane containing the vacancy, the same direction as the AFM spin direction. None of the NN bond lengths decreased more than 0.125 Å. The reason for our concern with the change in NN bond lengths will become more evident in the next section where we consider the monoclinic vacancy case. Finally, we note that the displacement vectors nearest the vacant site have the form [0, u_y, $\pm u_y$] in the $x = 0$ plane, and [0, $\pm u_y$, 0] or [0, 0, $\pm u_y$] in the adjacent parallel (100) planes. This displacement field retains the fourfold symmetry around the x axis and, therefore, corresponds to a displacement field of tetragonal symmetry. The displacement field of the monoclinic vacancy case, defined earlier, differs considerably from the tetragonal vacancy case.

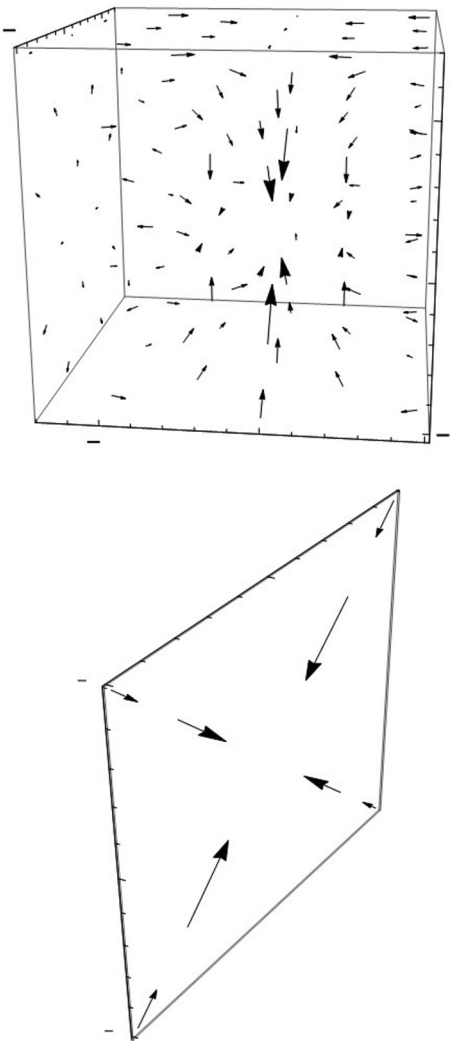

FIG. 2. Top shows a vector field plot of the displacement vectors after relaxation in the fcc Pu lattice containing a tetragonal vacancy at [0, 0, 0]. The length of the vectors have been scaled by a factor of 10. Bottom shows displacement vectors associated with atoms whose NN bond lengths have decreased by >0.1 Å. These vectors lie in the (100) plane containing the vacant site and show that the displacement field has tetragonal symmetry.

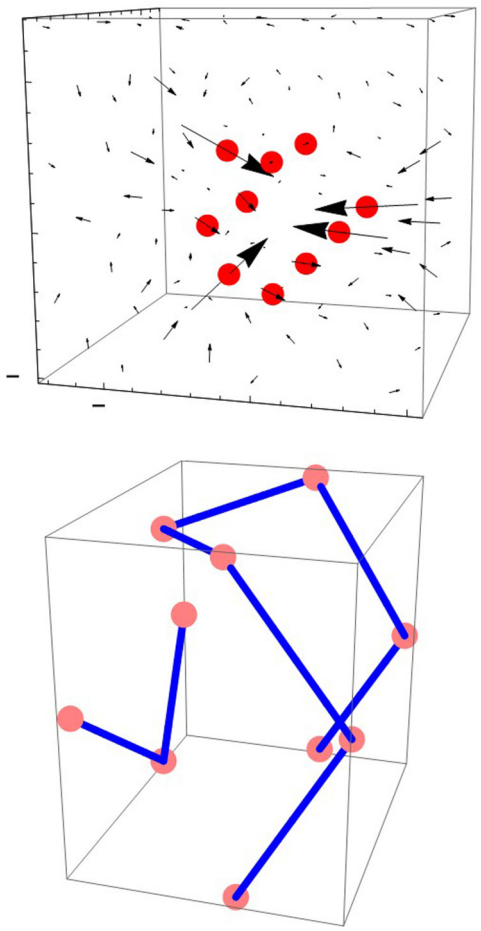

FIG. 3. Vector field plot showing the displacement field surrounding the monoclinic vacancy (top). The magnification factor is 5. Ten NN atoms surrounding the monoclinic vacancy are colored red and the blue lines are bonds between these atoms where bond lengths are in the range of 2.70 to 2.85 Å (bottom). Four of these atoms, in a tetrahedral arrangement, have undergone the largest displacements.

Figure 3 shows a vector field plot of the displacements for the monoclinic vacancy field, with a magnification factor of 5. The largest displacements are again associated with four atoms that are NNs to the vacancy. However, these four atoms do not lie in a single plane but rather form the corners of a tetrahedron and the displacement vectors are considerably larger than in Fig. 2, and are not directed toward the vacant site. Furthermore, the bonds between the ten atoms surrounding the vacancy (shown in red in Fig. 3) have reduced their NN distances substantially and these ten atoms and their connecting bonds are also shown in Fig. 3. The geometric arrangement of these atoms has low symmetry, only one mirror plane, and, therefore, possesses monoclinic symmetry.

The short NN bonds appearing as the blue connecting lines in Fig. 3 have bond lengths ranging from 2.70 to 2.85 Å, all considerably shorter than the 3.20 Å NN bond length in the perfect fcc Pu lattice. Furthermore, these bond lengths are comparable to the short NN bond lengths in α-Pu. In the paper by Hirth *et al.* [40], a table of NN bond lengths in α-Pu lists short bonds in the range of 2.60 to 2.80 Å. The arrangement of atoms surrounding the vacant site in the monoclinic vacancy case shown in Fig. 3 is consistent with both the monoclinic symmetry and bond lengths characteristic of α-Pu. The displacement field results above for the tetragonal and monoclinic vacancy imply an anisotropic bond strength in the nearest-neighbor atoms to the vacancies as revealed by these low-symmetry distortions. The bonding strength for pure δ-Pu (no defects) in the nearest-neighbor shell has been calculated with DFT and SOC to be highly anisotropic, resulting in lower-symmetry structures [41]. Even though our current calculations do not include SOC, we are still able to detect low-symmetry distortions associated with monovacancies, suggesting that neglecting SOC for defect calculations in δ-Pu may give qualitatively similar results.

To further understand the interrelated roles of magnetism and electronic structure underlying these unique structures, the $5f$ and $6d$ densities of states are shown for the tetragonal and

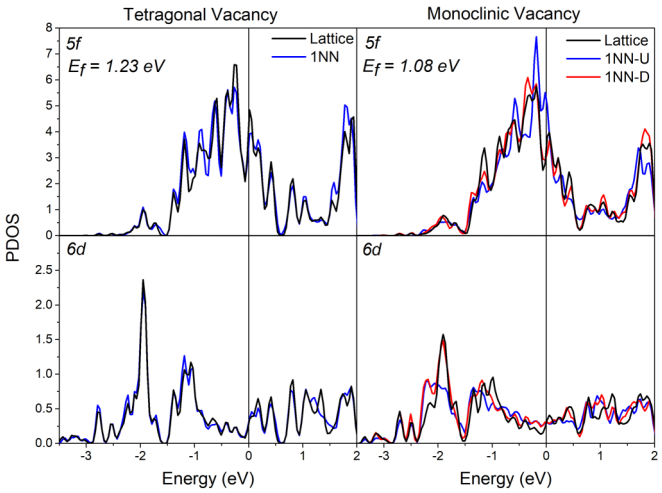

FIG. 4. Partial density of states of the $5f$ and $6d$ states for spin-up (1NN-U) and spin-down (1NN-D) Pu atoms that are nearest-neighbors and far (Lattice) from a tetragonal (left) and monoclinic (right) Pu vacancy.

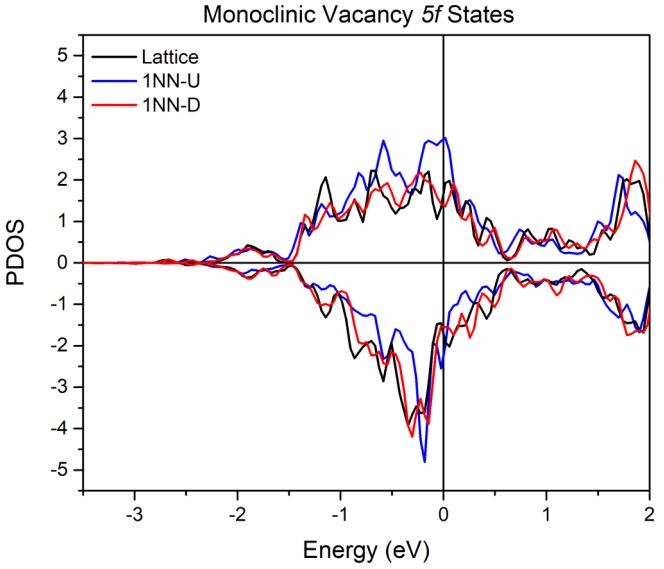

FIG. 5. Spin projection of the $5f$ partial density of states for spin-up (1NN-U) and spin-down (1NN-D) Pu atoms that are nearest-neighbors and far (Lattice) from the monoclinic vacancy.

monoclinic monovacancies. To this point as seen in Fig. 4, the total $5f$ PDOS are shown for a spin-up (1NN-U) and spin-down (1NN-D) Pu atom that is nearest-neighbor distance to the monovacancy, and a host lattice Pu atom that is noninteracting with the vacancy (lattice). From the PDOS for the tetragonal vacancy there is very little difference in the $5f$ and $6d$ states between a Pu atom that is near or far from the vacancy, concluding that a vacancy does not affect any of the valence electronic states. However, the PDOS for the monoclinic vacancy shows that a 1NN-U Pu atom within the monoclinic structure shows a $5f$ intensity increase right at the Fermi energy. Due to the increase and shift of $5f$ states and the known strong $5f$-$6d$ coupling in the actinides [42,43], there is a spectral shift of the $6d$ states to decrease in intensity, thus uncoupling the $5f$-$6d$ states. Recovery of local lattice distortions due to a defect has been postulated to occur by increasing the $5f$-$6d$ hybridization, thus strengthening the bonds in fcc PuSc alloys [44]. The spin projection of the $5f$ partial density of states (Fig. 5) illustrates that the $5f$ state at the Fermi energy is due to the spin components, which implies that the stabilization of the monoclinic vacancy is not via electronic density, but rather is spin-density dependent. Furthermore, the PDOS for a 1NN-U versus 1NN-D atom differs, where the 1NN-D PDOS yields a similar PDOS to a Pu atom that is not interacting with the defect (i.e., an atom in the perfect fcc lattice). This behavior suggests that the supercell excess spin-up density local to the vacancy must be adjusted to accommodate this heterogeneous configuration and the system accomplishes this total-energy minimization by exciting a local $5f$ state. This difference in PDOS between the 1NN-U and 1NN-D atoms arises due to the local bonding. The 1NN-U Pu atoms do not fully interact with the lattice, as there only exist three long bonds (3.0–3.10 Å) to surrounding lattice atoms, whereas the 1NN-D Pu atoms are fully interacting with the existing NN shell as there are nine long bonds ranging from the NN shell distance of 3.20 Å. Comparing to α-Pu, there are eight nonequivalent atomic sites, and these sites have varying short and long bonds. Site 8 has 13 long bonds in the structure (3.19–3.71 Å) and three short bonds (2.76–2.78 Å), while site 1 has five short bonds (2.57–2.76 Å) and seven long bonds (3.21–3.71 Å) [40,45]. These sites in α-Pu have been calculated to have a more localized and delocalized PDOS, respectively [46]. Thus, the 1NN-U Pu atoms have an increased spectral density at the Fermi energy, because the bonds have increased beyond the 3.20 Å NN distance for the δ-Pu lattice. This indicates that the local configuration involving a monoclinic vacancy within the δ matrix acts with α-like electronic properties as observed within the broader context of AFM Pu allotropic models [27].

The relative charge density and spin-density differences ($\Delta\rho$) are plotted in Fig. 6 and show the spatial distribution of the charge density and unpaired spin densities, respectively,

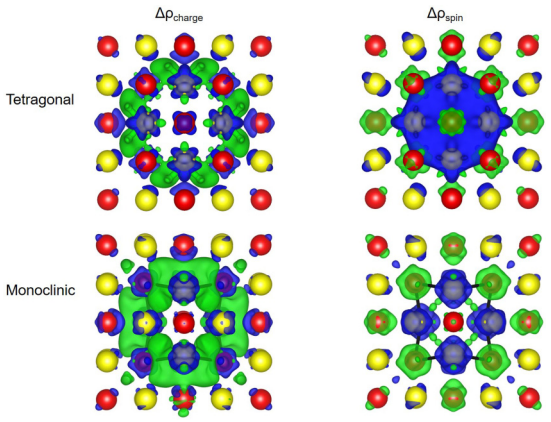

FIG. 6. Relative charge density difference and spin density difference for the tetragonal (top) and monoclinic (bottom) vacancy. Green indicates charge or spin accumulation (positive) and blue is charge or spin depletion (negative) with an isosurface level of $0.046\,e^{-}/Å^{3}$ and $0.046\,\mu_B/Å^{3}$.

TABLE I. Partial charges and spin magnetization for the eight Pu atoms with short bonds participating in the monoclinic structure around the vacancy and for the nonparticipating atoms (Lattice).

		Charge (e^-)		Spin (μ_B)	
Spin orientation	Atom	$5f$	$6d$	$5f$	$6d$
Up	1	5.307	1.386	4.537	0.180
	2	5.309	1.389	4.531	0.179
	3	5.303	1.379	4.550	0.182
	4	5.300	1.374	4.559	0.183
Down	5	5.356	1.545	−4.349	−0.139
	6	5.355	1.546	−4.348	−0.140
	7	5.349	1.534	−4.371	−0.143
	8	5.352	1.541	−4.357	−0.142
Up	Lattice	5.257	1.345	4.639	0.208
Down	Lattice	5.257	1.349	−4.638	−0.208

in the relaxed structure. The equation used to calculate these differences is

$$\Delta\rho = \rho_{\text{total}} - \rho_{\text{lattice}} - \rho_{\text{spin-up}} - \rho_{\text{spin-dn}} \quad (2)$$

where ρ_{total} is the total charge or spin density of the defective lattice, ρ_{lattice} is the charge density or spin density of the defective lattice without the nearest-neighbor spin-up and spin-down atoms to the vacancy, and $\rho_{\text{spin-up}}$ and $\rho_{\text{spin-dn}}$ are the charge density or spin density of the nearest-neighbor spin-up and spin-down atoms to the vacancy, respectively.

From the charge density difference there is noticeable charge buildup between the bonds in the monoclinic structure versus the tetragonal vacancy. One Pu atom that has NN bond length of 2.99 Å also exhibits the onset of charge buildup with a NN Pu atom within the local distortion, even though the bond length is greater than our defined short bond length, but less than the NN bond length in the δ lattice. Table I shows the calculated partial charges and spin for the individual Pu atoms that are in the local distortion. The average Pu atom in the cell (that is not participating in the local distortion around the vacancy) has a partial $5f$ and $6d$ charge of $5.257e^-$ and $1.347e^-$, respectively, and for the partial $5f$ and $6d$ spin magnitude of $4.639\mu_B$ and $0.208\mu_B$, respectively. These values are nearly the same as in the perfect fcc lattice where the partial $5f$ and $6d$ charges are $5.265e^-$ and $1.352e^-$, respectively, and the partial $5f$ and $6d$ spin magnitudes are $4.638\mu_B$ and $0.202\mu_B$, respectively. Comparing these numbers to the atoms in the local distortion of the monoclinic vacancy (Table I), there is more of an increase in the $5f$-$6d$ partial charge density, but there is a net increase in positive magnetization for the 1NN-D atoms, which overall decreases the magnitude of the magnetization. This is shown in the spin-density difference plot (Fig. 6, bottom) as there is an accumulation of spin density for the 1NN-D atoms and depletion of spin density for the 1NN-U Pu atoms lowers the magnitude of the magnetization. The decrease in the spin moment magnitude for the atoms in the monoclinic distortion also agrees well with the fact that atoms in α-Pu have relatively smaller spin moment magnitudes than atoms in δ-Pu [27]. This interplay between the $5f$-$6d$ spatial and spin wave-function densities reveals the implicit nature of electronic correlations in this hybridized system.

For the tetragonal vacancy this is not the case as the spin-density difference plot (Fig. 6, top) indicates that there is a collective loss of magnetization from the 1NN-U atoms within the interstitial region between lattice sites. Only the four 1NN-D atoms that participate in the tetragonal distortion (discussed above) have a slight relative local decrease or absolute increase in the $5f$ spin-density magnetization to $-4.577\mu_B$, but overall the partial charge and spin are similar to the perfect lattice.

IV. DISCUSSION

For the dilute limit of a monovacancy in δ-Pu, the DFT calculated tetragonal vacancy appears to acquire its form from the mechanical instability of the AFM structure and low shear elastic modulus of the δ-Pu lattice. When taken in addition to the absence of impact to the $5f$ and $6d$ states between a Pu atom that is near or far from the vacancy, this response once again suggests that the sustained fcc metallic behavior of the atoms involved in this defect even after ionic relaxation. However, this interplay between the $5f$-$6d$ states influences not only the local charge density but also the spin density, thus facilitating the stabilization of the local distortion around the vacancy becoming evident. In the case of the monoclinic vacancy, the $5f$-$6d$ states influences on the local charge density and the spin density are obvious. An increase in the d character in a spin-down atom allows for further coupling with the $5f$ states, which in turn decreases the d character in a spin-up Pu atom followed by a decoupling of the $5f$ states, enabling a shift towards the Fermi energy. The collective increase of the charge density, the decrease of the magnitude of the spin density, and the decrease of bond lengths in the monoclinic structure imply an attractive interaction within the structure, which strongly suggests covalency. Covalency in α-Pu has been postulated due to the measured high shear/bulk moduli ratio and low Poisson ratio [47,48]. This observation has been explained by the variation of interatomic distances resulting in a simultaneously delocalized/localized nature of the eight nonequivalent sites. The complicated nature of the α structure exhibits a dependence on directional bonding that weakens with increasing electron correlations, a Peierls distortion for the low-symmetry crystal structure, and possibly a magnetically frustrated system [46,49,50], but further studies are needed to fully understand α-Pu. All in all, the monovacancy induces local distortions that resemble low-symmetry Pu-phases in the fcc δ matrix.

V. CONCLUSIONS

In conclusion, the complexity of $5f$ electrons in Pu and radiation damage is still unexplored territory, highlighted by this study of the existence of local displacements that depart markedly from those typical of a vacancy in other simple fcc metals. We have calculated a ground-state structure for a monovacancy that has local distortions of Pu short bonds that only bind with antiparallel spins, comparable to the α phase. This structure is stabilized by the shifting of spin density of the $5f$ electrons, thus emphasizing the interplay between atomic spin moments as an additional degree of freedom that correspondingly influences charge density valence state composition. This energy minimization pathway has been

extremely advantageous to our study of defects in Pu as it has allowed the system to adopt locally the low-symmetry ground-state structure of Pu. Our understanding of defects in Pu is still in an exploratory phase, and as we begin to calculate interesting and unusual point defects we may begin to revolutionize a newfound understanding of radiation damage in Pu materials.

ACKNOWLEDGMENTS

We would like to acknowledge the Laboratory Directed Research and Development program at Los Alamos National Laboratory (LANL) for supporting the research associated with Project No. 20150057DR and Nuclear Survivability C7. Computational support was provided by LANL Institutional Computing project.

[1] A. C. Damask and G. J. Dienes, *Point Defects in Metals* (Gordon and Breach, New York, 1963).

[2] A. Kubota, W. Wolfer, S. Valone, and M. Baskes, Collision cascades in pure δ-plutonium, J. Comput.-Aided Mater. Des. **14**, 367 (2007).

[3] M. Robinson, S. D. Kenny, R. Smith, M. T. Storr, and E. McGee, Simulating radiation damage in δ-plutonium, Nucl. Instrum. Methods Phys. Res., Sect. B **267**, 2967 (2009).

[4] V. V. Dremov, F. A. Sapozhnikov, S. I. Samarin, D. G. Modestov, and N. E. Chizhkova, Monte Carlo+molecular dynamics modeling of radiation damages in Pu, J. Alloys Compd. **444–445**, 197 (2007).

[5] M. I. Baskes, Atomistic model of plutonium, Phys. Rev. B **62**, 15532 (2000).

[6] A. V. Karavaev, V. V. Dremov, and G. V. Ionov, Atomistic simulations of dislocation dynamics in δ-Pu-Ga alloys, J. Nucl. Mater. **496**, 85 (2017).

[7] S. C. Hernandez, F. J. Freibert, and J. M. Wills, Density functional theory study of defects in unalloyed δ-Pu, Scr. Mater. **134**, 57 (2017).

[8] P. Söderlind, Ambient pressure phase diagram of plutonium: A unified theory for α-Pu and δ-Pu, Europhys. Lett. **55**, 525 (2001).

[9] J. C. Lashley, A. Lawson, R. J. McQueeney, and G. H. Lander, Absence of magnetic moments in plutonium, Phys. Rev. B **72**, 054416 (2005).

[10] S. C. Hernandez, D. S. Schwartz, C. D. Taylor, and A. K. Ray, Ab initio study of gallium stabilized δ-plutonium alloys and hydrogen-vacancy complexes, J. Phys.: Condens. Matter **26**, 235502 (2014).

[11] B. Maiorov, J. B. Betts, P. Söderlind, A. Landa, S. C. Hernandez, T. A. Saleh, F. J. Freibert, and A. Migliori, Elastic moduli of δ-Pu239 reveal aging in real time, J. Appl. Phys. **121**, 125107 (2017).

[12] A. Migliori, P. Söderlind, A. Landa, F. J. Freibert, B. Maiorov, B. J. Ramshaw, and J. B. Betts, Origin of the multiple configurations that drive the response of δ-plutonium's elastic moduli to temperature, Proc. Natl. Acad. Sci. USA **113**, 11158 (2016).

[13] M. Janoschek, P. Das, B. Chakrabarti, D. L. Abernathy, M. D. Lumsden, J. M. Lawrence, J. D. Thompson, G. H. Lander, J. N. Mitchell, S. Richmond *et al.*, The valence-fluctuating ground state of plutonium, Sci. Adv. **1**, e1500188 (2015).

[14] P. Söderlind, F. Zhou, A. Landa, and J. Klepeis, Phonon and magnetic structure in δ-plutonium from density-functional theory, Sci. Rep. **5**, 15958 (2015).

[15] M. Janoschek, G. Lander, J. Lawrence, E. Bauer, M. Lumsden, D. Abernathy, and J. Thompson, Comments on "Phonon and magnetic structure in δ-plutonium from density-functional theory" by P. Söderlind *et al.*, arXiv:1602.01781.

[16] M. Janoschek, G. Lander, J. M. Lawrence, E. D. Bauer, J. C. Lashley, M. Lumsden, D. L. Abernathy, and J. D. Thompson, Relevance of Kondo physics for the temperature dependence of the bulk modulus in plutonium, Proc. Natl. Acad. Sci. USA **114**, E268 (2017).

[17] A. Migliori, P. Söderlind, A. Landa, F. J. Freibert, B. Maiorov, B. J. Ramshaw, and J. B. Betts, Reply to Janoschek *et al.*: The excited δ-phase of plutonium, Proc. Natl. Acad. Sci. USA **114**, E269 (2017).

[18] S. K. McCall, M. J. Fluss, B. W. Chung, M. W. McElfresh, D. D. Jackson, and G. F. Chapline, Emergent magnetic moments produced by self-damage in plutonium, Proc. Natl. Acad. Sci. USA **103**, 17179 (2006).

[19] P. E. Blöchl, Projector augmented-wave method, Phys. Rev. B **50**, 17953 (1994).

[20] G. Kresse and J. Hafner, *Ab initio* molecular dynamics for liquid metals, Phys. Rev. B **47**, 558(R) (1993).

[21] G. Kresse and J. Hafner, *Ab initio* molecular-dynamics simulation of the liquid-metal–amorphous-semiconductor transition in germanium, Phys. Rev. B **49**, 14251 (1994).

[22] G. Kresse and J. Furthmüller, Efficient iterative schemes for ab initio total-energy calculations using a plane-wave basis set, Phys. Rev. B **54**, 11169 (1996).

[23] G. Kresse and J. Furthmüller, Efficiency of ab-initio total energy calculations for metals and semiconductors using a plane-wave basis set, Comput. Mater. Sci. **6**, 15 (1996).

[24] J. P. Perdew, K. Burke, and M. Ernzerhof, Generalized Gradient Approximation Made Simple, Phys. Rev. Lett. **77**, 3865 (1996).

[25] J. P. Perdew, K. Burke, and M. Ernzerhof, Generalized Gradient Approximation Made Simple [Phys. Rev. Lett. **77**, 3865 (1996)], Phys. Rev. Lett. **78**, 1396 (1997).

[26] K. T. Moore and G. van der Laan, Nature of the $5f$ states in actinide metals, Rev. Mod. Phys. **81**, 235 (2009).

[27] P. Söderlind and B. Sadigh, Density-Functional Calculations of α, β, γ, δ, δ' and $\in$ Plutonium, Phys. Rev. Lett. **92**, 185702 (2004).

[28] G. Robert, A. Pasturel, and B. Siberchicot, Vacancy formation in δ-plutonium: A density-functional study in the generalized gradient approximation, Europhys. Lett. **71**, 412 (2005).

[29] P. Söderlind, Quantifying the importance of orbital over spin correlations in δ-Pu within density-functional theory, Phys. Rev. B **77**, 085101 (2008).

[30] P. Söderlind, A. Landa, and B. Sadigh, Density-functional investigation of magnetism in δ-Pu, Phys. Rev. B **66**, 205109 (2002).

[31] P. Söderlind, A. Landa, B. Sadigh, L. Vitos, and A. Ruban, First-principles elastic constants and phonons of δ-Pu, Phys. Rev. B **70**, 144103 (2004).

[32] P. Söderlind and A. Landa, Theoretical confirmation of Ga-stabilized anti-ferromagnetism in plutonium metal, J. Nucl. Mater. **448**, 310 (2014).

[33] J. Jacquemin and R. Lallement, Length variations of the α, β and delta phases of plutonium due to self irradiation at 1.4 deg K and 4.2 deg K, in *Proceedings of the Fourth International Conference on Plutonium and Other Actinides*, edited by W. N. Miner (Metallurgical Society of the American Institute of Mining, Metallurgical and Petroleum Engineers, New York, 1970), pp. 616–622.

[34] D. L. Clark, S. S. Hecker, G. D. Jarvinen, and M. P. Neu, in *The Chemistry of the Actinide and Transactinide and Elements* (Springer, Dordrecht, 2006), Chap. 7, p. 813.

[35] C. G. Van de Walle and J. Neugebauer, First-principles calculations for defects and impurities: Applications to III-nitrides, J. Appl. Phys. **95**, 3851 (2004).

[36] S. M. Foiles, M. I. Baskes, and M. S. Daw, Embedded-atom-method functions for the fcc metals Cu, Ag, Au, Ni, Pd, Pt, and their alloys, Phys. Rev. B **33**, 7983 (1986).

[37] F. J. Freibert, D. E. Dooley, and D. A. Miller, Formation and recovery of irradiation and mechanical damage in stabilized δ-plutonium alloys, J. Alloys Compd. **444–445**, 320 (2007).

[38] K. Momma and F. Izumi, VESTA 3 for three-dimensional visualization of crystal, volumetric and morphology data, J. Appl. Crystallogr. **44**, 1272 (2011).

[39] C. Teodosiu, *Elastic Models of Crystal Defects* (Springer, Berlin, 1982).

[40] J. P. Hirth, J. N. Mitchell, D. S. Schwartz, and T. E. Mitchell, On the fcc→monoclinic martensite transformation in a Pu-1.7 at.% Ga alloy, Acta Mater. **54**, 1917 (2006).

[41] K. T. Moore, P. Söderlind, A. J. Schwartz, and D. E. Laughlin, Symmetry and Stability of δ Plutonium: The Influence of Electronic Structure, Phys. Rev. Lett. **96**, 206402 (2006).

[42] R. Jullien, E. G. d'Agliano, and B. Coqblin, Hybridized non-degenerate $6d$ and $5f$ virtual-bound-states model for actinides metals, Phys. Rev. B **6**, 2139 (1972).

[43] R. Jullien, E. Galleani d'Agliano, and B. Coqblin, A simple model for the study of magnetism in transition-based alloys with actinide impurities, J. Low Temp. Phys. **10**, 685 (1973).

[44] J. P. Zanghi, D. Calais, and M. Boidron, Contraction par autoirradiation a 4,2 K de la phase δ cubique a faces centrées du plutonium, J. Nucl. Mater. **62**, 105 (1976).

[45] W. Zachariasen and F. H. Ellinger, The crystal structure of alpha plutonium metal, Acta Crystallogr. **16**, 777 (1963).

[46] J.-X. Zhu, R. C. Albers, K. Haule, G. Kotliar, and J. M. Wills, Site-selective electronic correlation in α-plutonium metal, Nat. Commun. **4**, 2644 (2013).

[47] A. Migliori, C. Pantea, H. Ledbetter, I. Stroe, J. B. Betts, J. N. Mitchell, M. Ramos, F. Freibert, D. Dooley, S. Harrington *et al.*, Alpha-plutonium's polycrystalline elastic moduli over its full temperature range, J. Acoust. Soc. Am. **122**, 1994 (2007).

[48] I. Stroe, J. B. Betts, A. Trugman, C. H. Mielke, J. N. Mitchell, M. Ramos, F. J. Freibert, H. Ledbetter, A. Migliori *et al.*, Polycrystalline gamma-plutonium's elastic moduli versus temperature alpha-plutonium's polycrystalline elastic moduli over its full temperature range, J. Acoust. Soc. Am. **127**, 741 (2010).

[49] P. Söderlind, O. Eriksson, B. Johansson, J. Wills, and A. Boring, A unified picture of the crystal structures of metals, Nature (London) **374**, 524 (1995).

[50] S. C. Hernandez, A. K. Ray, and C. D. Taylor, Quantum size effects in α-plutonium (020) surface layers, Solid State Commun. **172**, 29 (2013).